

Geochemical identification of impactor for Lonar crater, India

Saumitra MISRA^{1, 5, 6*}, Horton E. NEWSOM¹, M. SHYAM PRASAD², John W. GEISSMAN³, Anand DUBE⁴,
and Debashish SENGUPTA⁵

¹Institute of Meteoritics and Department of Earth and Planetary Sciences, MSC03 2040, 1 University of New Mexico,
Albuquerque, New Mexico 87131, USA

²National Institute of Oceanography, Dona Paula, Goa-403004, India

³Department of Earth and Planetary Sciences, MSC03 2040, 1 University of New Mexico, Albuquerque, New Mexico 87131, USA

⁴P 147/3, Janak Road, Kolkata-700 029, India

⁵Department of Geology and Geophysics, Indian Institute of Technology, Kharagpur-721302, India

⁶Present address: School of Geological Sciences, University of Kwazulu-Natal, Durban-4000, South Africa

*Corresponding author. E-mail: misrasaumitra@gmail.com

(Received 11 October 2008; revision accepted 12 April 2009)

Abstract—The only well-known terrestrial analogue of impact craters in basaltic crusts of the rocky planets is the Lonar crater, India. For the first time, evidence of the impactor that formed the crater has been identified within the impact spherules, which are ~0.3 to 1 mm in size and of different aerodynamic shapes including spheres, teardrops, cylinders, dumbbells and spindles. They were found in ejecta on the rim of the crater. The spherules have high magnetic susceptibility (from 0.31 to 0.02 SI-mass) and natural remanent magnetization (NRM) intensity. Both NRM and saturation isothermal remanent magnetization (SIRM) intensity are ~2 Am²/kg. Demagnetization response by the NRM suggests a complicated history of remanence acquisition. The spherules show schlieren structure described by chains of tiny dendritic and octahedral-shaped magnetite crystals indicating their quenching from liquid droplets. Microprobe analyses show that, relative to the target basalt compositions, the spherules have relatively high average Fe₂O₃ (by ~1.5 wt%), MgO (~1 wt%), Mn (~200 ppm), Cr (~200 ppm), Co (~50 ppm), Ni (~1000 ppm) and Zn (~70 ppm), and low Na₂O (~1 wt%) and P₂O₅ (~0.2 wt%). Very high Ni contents, up to 14 times the average content of Lonar basalt, require the presence of a meteoritic component in these spherules. We interpret the high Ni, Cr, and Co abundances in these spherules to indicate that the impactor of the Lonar crater was a chondrite, which is present in abundances of 12 to 20 percent by weight in these impact spherules. Relatively high Zn yet low Na₂O and P₂O₅ contents of these spherules indicate exchange of volatiles between the quenching spherule droplets and the impact plume.

INTRODUCTION

Meteoritic impact is an important geologic process in shaping planetary surfaces (Shoemaker 1977; French 1998), but there are few terrestrial analogues that help understand impact craters on planets with basaltic crusts (Grieve 1987; Earth Impact Database 2007). The best studied and fully accessible one is the Lonar crater (centered at 19°59'N, 76°31'E) in India (Nayak 1972; Fredriksson et al. 1973; Rao and Bahalla 1984; Ghosh and Bhaduri 2003; Kumar 2005) (Fig. 1). This crater was excavated in Deccan basalt, the bulk of which erupted near the Cretaceous-Tertiary boundary at 65 Ma, with a slightly earlier pulse between 68 and 67 Ma (65 ± 0.9 Ma, Hofmann et al. 2000; also see Courtillot et al. 2000; and close to 67.4 ± 0.9 Ma, Pande et al. 2004; 64.7 ± 0.6 Ma,

Chernet et al. 2007). However, the duration of this flood basalt volcanism is controversial. Courtillot and Renne (2003) believed that the bulk of this basalt erupted in a very short interval of time, less than 1 Ma, around the Cretaceous-Tertiary boundary between ~66 and 65 Ma. Wignall (2001) suggested that the main peak of Deccan eruption briefly occurred across this boundary, with volcanic activity continuing to ~63 Ma.

The only other impact crater in basalt is the 20 km in diameter Logancha crater in Russia, about which little information is available at present (Feldman et al. 1983; Masaitis 1999). The Lonar crater has great importance and pertinence to the understanding of small craters on planets with basaltic crusts, including the Moon and Mars (e.g., Fredriksson et al. 1973; Kieffer et al. 1976; Hagerty and Newsom 2003; Newsom et al. 2007).

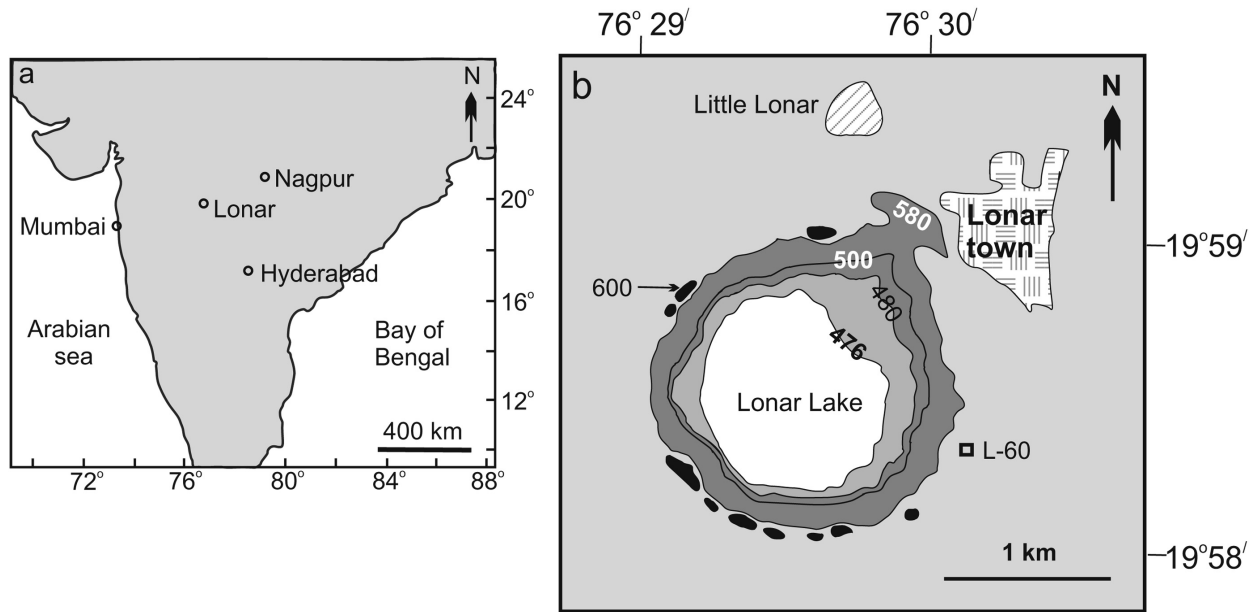


Fig. 1. Simplified maps of (a) India showing the position of Lonar crater, and (b) Lonar crater with topography (contours are shown in meters). The spherules (and impact melt breccia) site we investigated were obtained at the location marked with the black square and labeled L-60, which is close to the topographic rim.

The Lonar crater is a bowl-shaped simple impact structure with an average diameter of ~ 1830 m, a circularity of ~ 0.9 , and a depth of 120 m below the rim crest (Fredriksson et al. 1973; Fudali et al. 1980; Koeberl et al. 2004; Kumar 2005). The core of the depression is occupied by a shallow saline lake (pH: 9.5–10.0, Thakker and Ranade 2002), which has a maximum depth of ~ 5.5 m during monsoons (Chowdhury and Handa 1978), followed by ~ 100 m of unconsolidated sediments that overlie a brecciated and pulverized zone (Fredriksson et al. 1973). The brecciated and pulverized zone containing shocked and fractured basalt, and basalt powder extends to at least 400 m below the crater floor (Fudali et al. 1980). No evidence of Archaean basement rocks from beneath the basalts has been described in the deepest drill core (~ 344 m, Fredriksson et al. 1973) or ejecta of the Lonar crater. However, possible trace element (Rb, Ba, Th, U, and Pb) and isotopic (ϵ_{Nd} , radiogenic Sr and $^{207}\text{Pb}/^{204}\text{Pb}$) evidence of such material have been suggested (Chakrabarti and Basu 2006; Chakrabarti et al. 2006), although controversies about the source of these signatures exist (Misra 2006; Son and Koeberl 2007). About ~ 700 m north of the rim, there is another relatively small shallow, roughly triangular depression, known as the Little Lonar (Fig. 1b), which has a diameter of ~ 300 m and surrounded by a raised rim only along its southern and western margins. Master (1999) suggested that the Lonar crater and Little Lonar might have been formed together by near-simultaneous double impacts of fragments of the same bolide, but drilling into the structure revealed no evidence for this (Fredriksson 2000; personal communication) and no meteorites have been found associated with the Little Lonar structure. However, the absence of any meteorite

fragments at Lonar or Little Lonar could be due to either the disintegration of the impactor in the atmosphere (e.g., Boslough and Crawford 2008) or the rapid post-impact weathering of meteorite fragments, or both.

Thermoluminescence dating of three in-situ impact melt samples collected from northern, western, and eastern parts of the Lonar crater rim from within the ejecta blanket yielded a mean age of $52,000 \pm 6000$ yr for the Lonar crater (Sengupta et al. 1997). This age estimate is close to the fission-track age of Lonar impactites, which was less than 50,000 years (D. Lal, unpublished data; cf. Fredriksson et al. 1973). More recently, Storzer and Koeberl (2004) also reported an apparent fission track date of 15.3 ± 13.3 ka for three impact-glass samples from Lonar crater. The very high error of this date was the result of the low number of tracks counted. The sediments deposited in the saline lake within the Lonar crater were also dated using radiocarbon methods and yielded a date of 15–30 ka (unpublished data; see Fredriksson et al. 1979; Sengupta et al. 1997). As the lake sediments were contaminated by modern carbon, the radiocarbon dates obtained were interpreted as minimum ages of impact for the Lonar crater. Hence, if we accept the ~ 30 ka radiocarbon age estimate of the lake sediments as the minimum age of impact, Sengupta et al. (1997) average thermoluminescence date of ~ 52 ka for impact melts is perhaps close to the absolute age of the crater's formation.

Although studied since the late 19th century, (Gilbert 1896), the nature of the impactor for the Lonar crater has not been identified either in the field (Nayak 1972; Fredriksson et al. 1973; Fudali et al. 1980; Ghosh and Bhaduri 2003; Kumar 2005) or in geochemical studies (Nayak 1972;

Fredriksson et al. 1973; Kieffer et al. 1976; Stroube et al. 1978; Morgan 1978; Ghosh and Bhaduri 2003; Osaie et al. 2005; Chakbarti and Basu 2006; Son and Koeberl 2007). The lack of meteorite material at Lonar crater prompted several searches for siderophile element and/or platinum group geochemical signatures of an impactor (Morgan 1978; Ghosh and Bhaduri 2003; Osaie et al. 2005; Son and Koeberl 2007). For those craters where remnant projectile fragments are not preserved, analyses of Ni, Co, and PGEs of target rocks and impactites can still provide an indication of the type of impactors (Koeberl 1998, 2007; Grieve 1991). Morgan (1978) analyzed two Lonar target basalts and three impact-glasses with radiochemical neutron activation analysis and did not find any significant Ir enrichment. In his study, Lonar glasses were also found to be significantly depleted in Re (~7 times) and Se (~2.5 times) relative to parent basalts, which was attributed to a volatilization effect occurring during terrestrial impacts. The small depletions of Lonar impact glasses in Au (~27%) and Zn (~14%) were attributed to variations in target rock composition. On the basis of major and limited trace element data for target basalt and impact melts, Ghosh and Bhaduri (2003) and Ghosh (2003) suggested a cometary impact origin. Osaie et al. (2005) reported analytical data for target basalt, varieties of impact melts and spherules with negative results for siderophile enrichments and concluded that the impactor was perhaps non-chondritic or otherwise Ir-poor. Recently, Son and Koeberl (2007) reported detail analyses of 67 impact melt samples collected from the ejecta blanket around the crater rim, but no enrichment of any meteoritic component was seen. Kearsley et al. (2004), however, reported the presence of small (<10 μm) iron-nickel particles with a wide range of Fe/Ni ratios (0.02–14.4) within vesicles of Lonar impact melts, but it is not clear whether these fragments represent an indigenous component (may be reduced during impact) or an extraterrestrial contamination (Osaie et al. 2005). Further work by Son and Koeberl (2007), however, does not confirm any presence of iron-nickel particles within Lonar impact melts. Chakrabarti and Basu (2006) and Chakrabarti et al. (2006) generated Nd, Sr, and Pb isotopic data of Lonar target basalt and some impact breccia for the first time, but their study did not focus on the impactor's nature, and all of the impact breccia samples used by them were also of an uncertain origin (Misra 2006).

In the present paper, we report the discovery of submillimeter-sized impact spherules in the continuous ejecta blanket of Lonar crater. These spherules are unique in their chemistry and have high magnetic susceptibility and remanence intensity.

GEOLOGIC SETTING

The Deccan Traps, one of the largest volcanic provinces in the world, covers nearly 50,000 km² of west-central India (Fig. 1a) and overlies a basement ranging in age from Archean to Cretaceous (Mahoney 1988; Widdowson et al. 2000; Sheth

2007 and references therein). The trap, which is made up almost completely of evolved subalkaline tholeiitic basalts, except rare felsic and alkaline lavas along the rift zones and western coast, is the thickest (~2000 m) along the western coast of India, known as the Western Ghats, and continues further west onto the continental shelf. It thins progressively eastward and southeastward such that it has a thickness of 200 m or less along the eastern fringe of the lava province.

The stratigraphy of basalt flows exposed in and around the Lonar crater has been reinvestigated by Ghosh and Bhaduri (2003). There are six Deccan flows exposed in the region, each with a thickness between ~8 and 40 m, of which four lower flows are only exposed along the crater wall. The top-most two flows crop out away from the crater and may have not been present in the target area. These undeformed horizontal basalt flows show (a) cooling-related columnar joints where the column diameter varies from few cm to >1 m, and (b) sub-vertical fractures with orientation mostly in NW-SE to NNW-SSE directions, and a few in NE-SW direction (Kumar 2005). These fractures are broadly similar to the major fracture systems found in other parts of the Deccan volcanic province (Widdowson and Mitchell 1999). Each flow is separated from the next one by discontinuous marker horizons such as red and green colored palaeosols, chilled and vesicular margins, vugs filled with secondary material such as chlorite, zeolite, quartz, and brown limonite. In addition, chilled bottom and clinker to brecciated top with vesicular filling characterize most of the flows. Fresh, dense basalts are available only in the upper ~50 m of the crater wall, whereas below this level the flows are heavily weathered and friable (Fudali et al. 1980). Pre-crater black, dense, sticky humus-rich soil ~0.05 to 0.9 m thick is still preserved at places between the flows and the ejecta (Ghosh and Bhaduri 2003). All basalt flows have a common mineralogy and texture except some minor petrographic differences in the abundance of plagioclase phenocrysts, glass, and opaque minerals. The basalts are porphyritic with occasional phenocrysts of plagioclase and rare olivine set in a groundmass of plagioclase, augite, pigeonite, titanomagnetite, palagonite, and secondary minerals such as calcite, zeolite, chlorite, serpentine, and chlorophaeite (Ghosh and Bhaduri 2003). The Lonar basalts are relatively low-K tholeiitic within-plate basalt that are marginally enriched in Fe and Ca, and depleted in Mg and Al compared to average tholeiites of Irvine and Baragar (1971). They show limited compositional variation except for Cr, Ba, and volatile elements, which are more varied. (Osaie et al. 2005).

The weathered surface on the crater wall has an average slope of ~26° (Fudali et al. 1980) and is mostly covered by thick overburden or talus vegetation and surface weathering features. The rim of the crater rises ~30 m above the surroundings, and the crater floor lies ~90 m below the pre-impact surface. With the exception of the northeast part of the crater rim, there is a continuous ejecta blanket that extends outward to an average distance of ~700 m in all directions

except to the west where it extends a little more than 1 km (Misra et al. 2006a). This ejecta blanket has a very gentle slope of 2–6° away from the rim of the crater (Fudali et al. 1980), and consists of angular blocks of basalt of variable sizes cemented in very fine ejecta, the typical size of the blocks is measured up to ~5 m in diameter. The impact ejecta around the Lonar crater has three basic components (Ghosh and Bhaduri 2003): (a) an unshocked throw-out ejecta, (b) mixed shocked ejecta, and (c) shock-melted glass. The throw-out ejecta constitutes an almost continuous blanket over the target basalt extending up to 1.5 times the crater radii around the crater's rim. The exposures of mixed shocked ejecta and shock melts are more abundant around the crater within 0.5 crater radii from the crater's rim, where the latter directly overlie the former. The flows exposed in the crater's wall at the NE part of the crater's rim are offset by a listric fault, and three sets fracture systems (radial, concentric and conical) are exposed in the upper ~30 m of the crater's wall below the rim (Kumar 2005). All these structures were suggested to have been generated by meteoritic impact. Beyond the continuous ejecta around the crater's rim within a distance of ~3 km, Fudali et al. (1980) identified discontinuous patches of ejecta and large secondary craters.

SAMPLES AND ANALYTICAL TECHNIQUES

The spherules we studied were collected from the matrix material adjacent to in-situ pieces of centimeter-sized impact melt clasts recovered from a pit ~48 cm deep dug about 250 m southeast of the crater rim (GPS location: 19°58.356'N, 76°31.072'E) (Fig. 1b). Contamination is unlikely as the site has no evidence of any development. The fine-grained ($\geq 250 \mu\text{m}$ in size) samples of matrix material (weighing ~250 g) collected from the surfaces of these clasts were first cleaned, dried, and a hand-held magnet of 1400 gal (cm/s^2) strength was run over this material. The material attracted to the magnet included coarse-grained earthy particles, some titanomagnetite crystals, and about 100 submillimeter-sized spherules. The yield of these spherules amounts to ~0.4 spherule/gram of ejecta. The larger spherules were visible in the binocular microscope in both the magnetic and non-magnetic fractions. Fourteen such randomly selected submillimeter spherules were observed under the scanning electron microscope (SEM) (Fig. 2). Additionally, another 18 spherules (diameter range ~325–970 μm) were selected randomly for energy dispersive spectrometer (EDS) and electron probe microanalyser (EPMA) analyses, and the rest for measurements of magnetic susceptibility, basic rock magnetic properties and demagnetization response of the natural remanent magnetization (NRM).

The spherules under investigation were mounted in epoxy, grounded, and polished to expose their internal features for SEM and EPMA analyses. The SEM observations were carried out with a JEOL JSM-5800LV

instrument, at the National Institute of Oceanography, Goa, India. A JEOL 8200 electron microprobe at the University of New Mexico, Albuquerque, USA, was used for analysis of major oxides and some minor elements (Cr, Mn, Co, and Ni). The instrument was equipped with three conventional wavelength-dispersive (WD) spectrometers and two spectrometers with special capabilities for trace element analysis including an H type spectrometer and one equipped with a large PET crystal (PETL) crystal spectrometer. Quantitative analysis used a 15 μm broad beam, 15 keV accelerating voltage and 20 nA sample current, with ZAF correction routines. The calibration standards used were orthoclase (Al, Si, K), albite (Na), diopside (Mg, Ca), hematite (Fe), apatite (P), chromite (Cr), benitoite (Ti), and metals (Ni and Co). Long peak counting times up to 200 s were used to lower detection limits for Cr, Co, and Ni. Ni and Co were measured on a LiFH crystal on a JEOL "high intensity" or H-type spectrometer. The H-type spectrometer utilizes a reduced Rowland circle 120 mm in radius compared to the standard JEOL spectrometer that uses 140 mm Rowland circle. Therefore, the H-type spectrometer can provide an order of magnitude improvement in count rates for Ni (775 counts/s/nA on pure Ni compared to 86 cps/nA for a conventional spectrometer). The improved count rate, coupled with a 200 s measurement time, yields a 1-sigma detection limit of 80 ppm, although a more conservative detection limit at 2-sigma (160 ppm) could be used. A large PET crystal (PETL) on spectrometer 2 also improved the count rate on Cr by greater than 2.5 times over the conventional spectrometer. The precision of the minor element data at low abundances were verified by analyzing the NIST SRM 610 glass standard (Rocholl et al. 1997) and other standards before and after the spherule analyses. For example, Ni analyses of the NIST 610 sample before and after the analytical run gave a net of 3.7 counts per second and produced values of 417, 440, 408, and 401 ppm, all within 10% of the preferred value of 443 ppm (Rocholl et al. 1997) and well within the variation seen in the reported analyses of that standard. For cobalt, a correction was made for interference from iron. Detection limits for the minor and trace elements are Ti: 70 ppm, Mn: 90 ppm, Na: 140 ppm, K: 80 ppm, P: 30 ppm, Cr: 30 ppm, Co: 50 ppm, and Ni: 70 ppm. The one-sigma relative analytical uncertainty (standard deviation in percent) for the minor and trace elements on the Ni-rich samples are Ti: 1%, Mn: 5%, Na: 2%, K: 4%, P: 8%, Cr: 5%, Co: 13%, Ni: 4%.

At the University of New Mexico, a Kappabridge KLY-4S automated magnetic susceptibility instrument was used for magnetic susceptibility measurements. All remanence and additional rock magnetic measurements were made on a 2G Enterprises Model 760R superconducting rock magnetometer, equipped with DC squids and interfaced with an on line alternating field (AF) demagnetization

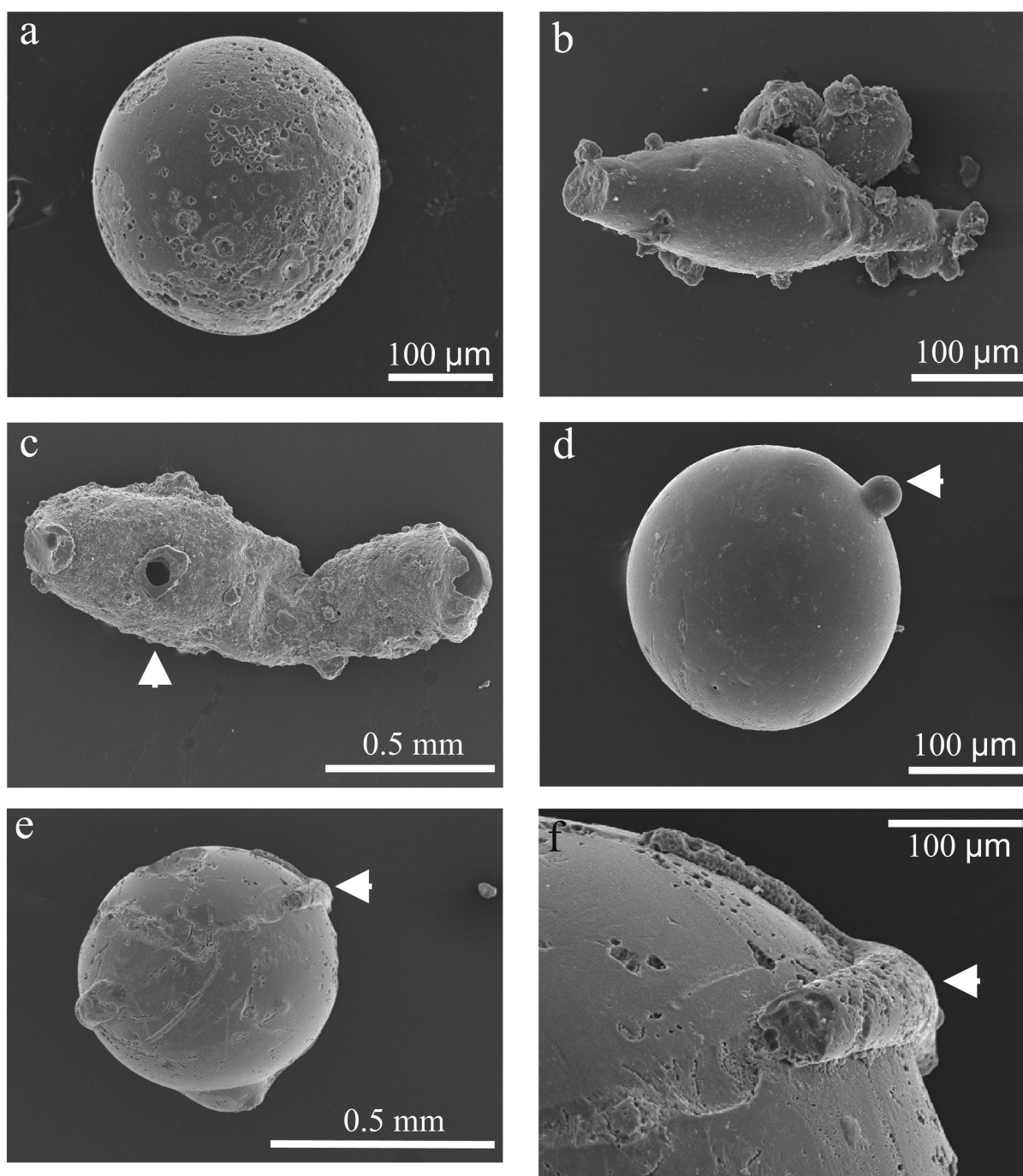


Fig. 2. SEM images of typical spherules from the Lonar ejecta blanket. a, d, e) Spherical shaped particles. b) Spindle shaped particle. c) Dumbbell shaped particle with a prominent vesicle noted by an arrow. d, e, f) The attached welded droplets (d) and drapings (e, f) indicated by arrows provide evidence for low-velocity impacts between the particles entrained in an impact-generated plume.

system. All experiments were conducted within a large volume, magnetically shielded space. For the Lowrie-Fuller tests (Johnson et al. 1975), anhysteretic remanent magnetization (ARM) was imparted using a peak alternating field of 95 mT in a DC bias field of 0.1 mT and isothermal remanent magnetization (IRM) was imparted with a DC field of 95 mT.

SPHERULE MORPHOLOGY

The impactites occurring within the Lonar crater's ejecta blanket are of two types (Osae et al. 2005): centimeter-sized (maximum up to ~30 cm) impact melt bombs (type "c" impactite in Osae et al. 2005) like the flädle of Ries crater, Germany (Hörz 1965) and millimeter-sized impact spherules

with a range of splash form shapes (type “a” impactite in Osae et al. 2005). These impact melt rocks and spherules have relatively low magnetic susceptibility and the latter particularly have highly vesicular surfaces with silica infillings in some cases.

SEM examination of external morphology of the newly discovered submillimeter-sized spherules with relatively high magnetic susceptibility show that these spherules have smooth surface texture and are dominantly spherical in shape, although teardrop, cylinder, dumbbell and spindle shapes are common (Figs. 2A–C). Some of the spherules have vesicles having silica infillings. Some spherules also have small adhering particles (Fig. 2D), which are compositionally similar to the host spherules. Interestingly, some of the spherules have draping on their surfaces (Figs. 2E and 2F), which have higher silica contents.

The polished sections of these spherules are generally free of voids. Out of the 18 spherules grounded and polished, only one contains an extensive vesicle rich-zone in one half of the grain (Fig. 3A). The other grains have few sparsely distributed vesicles or none. Therefore, the general absence of vesicles and smooth surface texture may be taken as characteristics of these submillimeter-sized spherules, which distinguish them from their larger counterparts (Osae et al. 2005).

BSE images of the internal structures of the submillimeter-sized spherules show that the spherules exhibit tiny iron oxide grains ($<2 \mu\text{m}$) with dendritic and octahedral shapes that are distributed in varying proportions along sub-parallel chains in schlieren structure (Figs. 3B–D). Although trains of minute cross-shaped titanomagnetite crystals were reported earlier in Lonar impact melt bombs (Fredriksson et al. 1973; Kieffer et al. 1976; Son and Koeberl 2007), we report the same features in impact spherules for the first time. Layers rich in subhedral equant to square-shaped iron oxide particles of variable width alternate with glassy layers that show flow banding (Fig. 3E). In rare instances, iron oxide grains form close irregular shape rings with individual crystals of the same in between (Fig. 3F). Only one submillimeter spherule contained an inclusion consisting of prismatic calcic plagioclase.

MAGNETIC PROPERTIES

Recently obtained geophysical data show circular- to semi-circular-shaped gravity and magnetic anomalies over the Lonar crater and its impactites of 2.5 mGal and 550 nT, respectively, which are very similar to the other impact craters of the world (Rajasekhar and Mishra 2005). These anomalies suggest that the impact had modified the magnetization vector and density of the target rock Deccan Traps to a depth of about 500–600 m below the surface, a distance some 0.3 to 0.35 times the diameter of the crater. The impact had remagnetized this region in the present day Earth’s magnetic field, demagnetizing the remnant magnetization of the Deccan Traps. Part of the brecciated zone below the crater

shows very high susceptibility of about 4.0×10^{-3} SI (reference).

In an extended abstract, Weiss et al. (2007) reported magnetic data from fläden and impact spherules recovered from the ejecta blanket around the rim of Lonar crater to test the hypothesis that these materials might have acquired a magnetization in an unusually strong (high paleointensity) field (Gattacceca and Rochette 2004). They reported that all glasses carried a natural remanent magnetization (NRM) with saturation isothermal remanent magnetization (SIRM) values of $\sim 2 \text{ A m}^{-1}$ (with saturation at about 300 mT), ratios of coercivity of remanence (H_{cr}) to coercivity (H_c) of ~ 2 , ratios of initial susceptibility to saturation remanence of ~ 0.007 , and no appreciable remanence anisotropy. Thermal demagnetization of relatively coarse glass samples showed maximum laboratory unblocking temperatures of $\sim 520 \text{ }^\circ\text{C}$. Ratios of NRM to SIRM for the small glasses were only 0.5 to 1.0×10^{-3} , while for the large glasses this ratio was twice as large. These ratios are nearly an order of magnitude smaller than those reported for Deccan basalt exposed at sites near the Lonar impact (Louzada et al. 2007).

The submillimeter-sized Lonar impact spherules examined in the present study have susceptibilities ranging from 0.31 to 0.02 (SI-mass), and NRM and SIRM intensities that are nearly equal and typically about $2 \text{ Am}^2/\text{kg}$. The larger, millimeter-sized spherules (Osae et al. 2005) are characterized by NRM intensities between 0.016 and $0.175 \text{ Am}^2/\text{kg}$, and susceptibilities between 1.3 and 2.5×10^{-4} SI-mass. For the millimeter-sized impact spherules, progressive alternating field (AF) demagnetization to 100+ mT typically reveals varying degrees of a curvilinear response rather than a single, discrete magnetization isolated over a wide range of peak fields (Figs. 4A–E). Intensities of anhysteretic remanent magnetization (ARM) acquired in a DC field of 0.05 mT are typically an order of magnitude lower than those of NRM suggesting a very effective process (e.g., possibly elevated ambient field at the time of impact, as explored by Weiss et al. 2007) of initially magnetizing the spherules. Further support for this is provided by SIRM intensities that are comparable to or at most only a factor of two higher than NRM intensities. A comparison of AF demagnetization response of NRM, ARM and SIRM show varied response but suggest high contribution by single-domain magnetite particles (Fig. 4F) (Johnson et al. 1975). The degree of magnetic particle interaction (Cisowski 1981) in the spherules is high, with the cross-over point at about 0.3 at a field of about 50 mT, slightly below typical coercivity of remanence (H_{cr}) values between 70 and 80 mT (Fig. 4G).

The magnetic properties of submillimeter-sized impact spherules, in particular the similarity in their high NRM and SIRM intensities, which is different from data on Lonar glasses reported by Weiss et al. (2007), and progressive demagnetization response, are consistent with a NRM that is dominated by a thermoremanent magnetization. This was likely to have been acquired rapidly while the orientation of individual impact spherules changed relative to the ambient

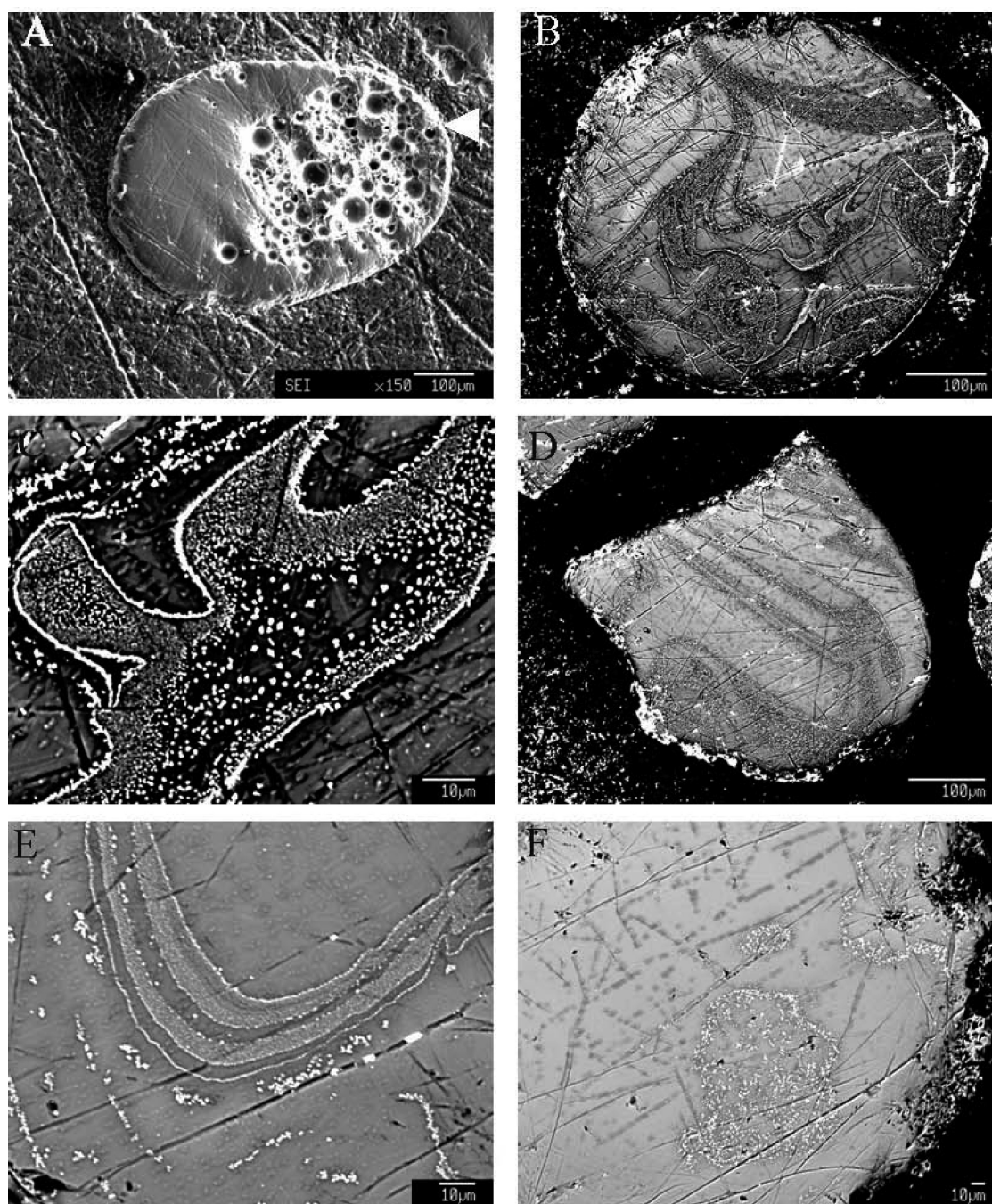


Fig. 3. Secondary and backscattered electron images of cross sections of submillimeter-sized, high magnetic susceptibility spherules in grain mounts. A) An unusual collection of vesicles is present in the interior of one spherule in a secondary electron image. B–F) Bands of iron oxides are seen in the backscattered electron images. The close-up in (C) is a portion of the spherule shown in (B).

field during magnetization blocking, possibly in a manner similar to that described by Weiss et al. (2007). The magnetic data are also consistent with additional evidence that the particles are quenched liquid droplets instead of condensates from an impact-generated hot vapor plume, including the presence of schlieren in the spherules (Figs. 2 and 3) and experimental evidence that condensates are more granitic in composition having higher SiO_2 , Na_2O , and K_2O , and

depleted FeO and CaO compared to target basalt (Yakovlev and Basilevsky 1994).

GEOCHEMISTRY

The analyses of the submillimeter-sized spherules show that these spherules are homogeneous in bulk chemistry. Microprobe analyses of both the melt-rich, and magnetite-

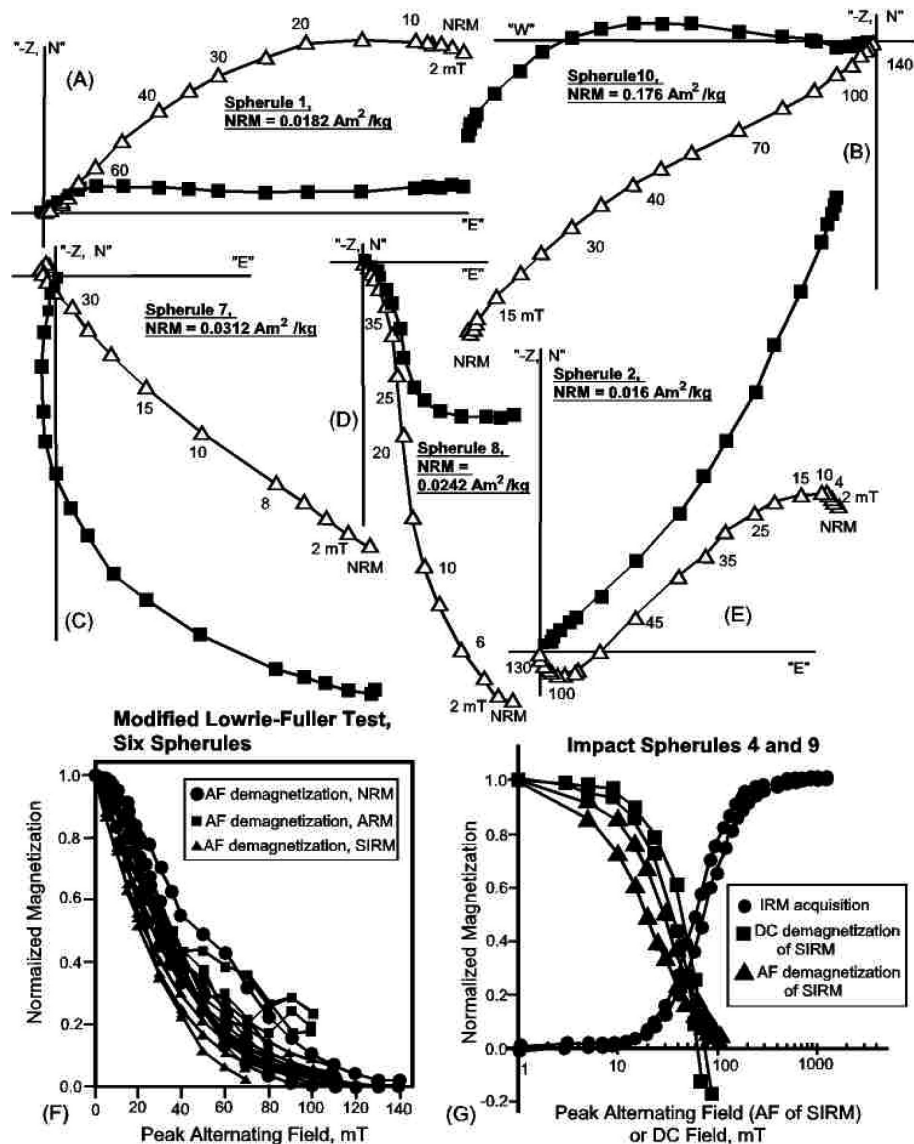


Fig. 4. Magnetic properties of mm-sized Lonar impact spherules. A–E) Examples of response to progressive AF demagnetization of mm-sized spherules. Orthogonal demagnetization diagrams (endpoint of the magnetization vector projected onto the horizontal [solid symbols] and vertical [open symbols] [specimen coordinates] planes) reveal a typical curvilinear response rather than the definition of one or more discrete components of magnetization isolated over a range of peak fields. F) Alternating field demagnetization response of NRM, ARM, and SIRM of six select mm-sized spherules. G) Comparison of IRM acquisition, direct field demagnetization of SIRM, and AF demagnetization of SIRM. (Cisowski 1981) of two select mm-sized impact spherules showing the strong magnetic interaction characteristic of the mm-sized spherules.

rich domains of these impact spherules (Fig. 3) show that these domains have overlapping average bulk compositions where the melt-rich areas show marginal enrichment in SiO_2 , and little, if any, distinctive difference in their minor element abundances (Appendix and Table 1). These spherules are distinct from the average target basalt by having relatively high Fe_2O_3 and MgO , low Na_2O , K_2O , and P_2O_5 , and distinctly higher Cr, Co, and Ni contents. The Ni content shows the largest variation from ~ 60 to 2500 ppm in these spherules. The bulk chemistry of the larger, millimeter-sized impact spherules is not available at present (Osae et al. 2005). The average major oxide composition of impact spherules of

Fredriksson et al. (1973), however, have relatively high FeO^T and MgO , which is comparable to the submillimeter-sized impact spherules in present study (Table 1).

In #Mg versus Ni space the target basalt and impact spherules show linear decreasing trends of different slopes for Ni with decreasing #Mg (Fig. 5a). The relatively steep trend for the submillimeter-sized impact spherules, however, is broadly defined and distinctly different from the sharply defined low-angle trend of target basalts. The impact melt bombs do not show any relative enrichment of Ni, and they form overlapping fields with target basalt. In Fe, Mg, and Cr plots against Ni, the submillimeter-sized impact spherules

show moderately well-defined increasing linear trends ($R^2 = 0.43$ to 0.64) with increasing Ni (Figs. 5b, 5d, 5e). The well-defined trend for target basalts in Ni versus Cr diagram ($R^2 = 0.86$) is also different from that of the impact spherules. In the Ni versus Mn diagram the submillimeter-sized impact spherules do not show any significant variation with increasing Ni but Mn content of these spherules is ~ 200 ppm higher than that of an average target basalt (Fig. 5c). The target basalt in this diagram show very high linear increase of Mn with little increase in Ni. In Ni versus Co plot (Fig. 5f), the submillimeter-sized impact spherules define an increasing trend for Co with increasing Ni, the trend, however, is very broadly defined ($R^2 = 0.23$). In these variation diagrams, the impact melt bombs and millimeter-sized large impact spherules (Osae et al. 2005) are always plotted together with the target basalts. In the Ni versus Zn plot (Fig. 5g) the target basalts, impact melt bombs and mm-sized spherules form a cluster, though the variation in Zn in the impact melt bombs from ~ 0 to 300 ppm is important. The submillimeter-sized spherules define a distinctly different decreasing trend for Zn with increasing Ni.

Osae et al. (2005), and Son and Koeberl (2007) suggested that the impact melt bombs and millimeter-sized larger impact spherules from the Lonar crater had target basalt-dominated chemistry and there was minimum fractionation of immobile elements (e.g., rare earth elements) between them. The target basalt, impact melt bombs and large millimeter-sized impact spherules in their study have very restricted Ni concentrations (≤ 200 ppm). The submillimeter-sized spherules newly identified in the present study, which also show target basalt-dominated bulk chemistry (Table 1), have much higher siderophile trace element (Cr, Co, Ni) contents. Explanations for this unusual chemistry of the submillimeter-sized spherules could include igneous fractionation, a contribution from mantle xenoliths, aqueous or hydrothermal weathering processes or the presence of meteorite material from the impactor.

Any common igneous process relating to genesis of target basalt and these impact spherules can be ruled out because they show distinctly different trends in #Mg versus Ni, and Ni versus Mn and Cr diagrams (Figs. 5a, 5c, 5e). Furthermore, these spherules cannot be mantle inclusions because they are not ultrabasic but basaltic in bulk composition similar to the target basalt (Table 2), and no mantle inclusions have been reported by the numerous studies on this area over many decades. The other plausible source of high Ni in the spherules would be enrichment in olivine, but olivine is rare in the Lonar basalts (Fredriksson et al. 1979), and no olivine inclusions are reported within these spherules either under microscope examination (Fredriksson et al. 1973) or in our BSE image analyses and microprobe study. Weathering and hydrothermal alteration of the ejecta blanket are the subjects of ongoing research (Misra et al. 2006b; Newsom et al. 2007). Osae et al. (2005), however, observed a very limited variation in As, Zn, Sb, Br, and Ce in the Lonar

samples collected mostly near the crater's rim and suggested that the effect of post-impact weathering was minimal. Limited hydrothermal activity at Lonar may have affected material retrieved as drill cores from the crater floor (Hagerty and Newsom 2003). It is also difficult to imagine that the immobile siderophile elements like Fe, Cr, Co, and Ni would be concentrated into these spherules by low-temperature hydrothermal solution active during weathering. Therefore, any observed variations in siderophile element and mobile element concentrations in the Lonar impactites in this study have genetic importance.

The region around the Lonar crater has a long history of human activity (Misra 2006), but an anthropogenic origin for these spherules is unlikely because the samples were obtained from within the ejecta from a depth of ~ 0.5 m in association with impact melt bombs. In addition, the typical splash shapes of the spherules (Fig. 2) suggest their rapid atmospheric chilling, an unlikely property for an anthropogenic deposit. Therefore, we proffer that contamination of impact-generated target basalt melt by impactor meteorite composition is the only possible explanation for the siderophile element compositions of these submillimeter-sized spherules (cf. Koeberl 1998, 2007).

It is well known that concentrations of the highly siderophile elements, including the platinum group elements (PGEs) and gold, can be a more sensitive indicator for meteorite components in impact melts and spherules than the siderophile elements Cr, Co, and Ni alone (e.g., Morgan et al. 1975; Gros et al. 1976; Palme et al. 1978, 1979; Tagle and Hecht 2006; cf. Koeberl 2007; McDonald et al. 2007). This is because the abundances of PGEs in chondrites and most iron meteorites are several orders of magnitude higher than those of the terrestrial target rocks (continental and oceanic). However, the abundances and ratios of siderophile elements can also be used for identification of meteoritic components if the meteoritic contribution in impactites is high (exceeding 0.1 weight percent) and the compositions of target rocks are well known (Koeberl 2007). Under these conditions, siderophile element chemistry can be used to distinguish between stony meteorites (chondrites) and iron meteorites, because chondrites have higher concentrations of Cr (typically about 0.26 weight percent) in comparison to iron meteorites with Cr concentrations that are much more variable, but typically about 100 times lower than those of chondrites. Chondrites also have high Ni/Cr and Co/Cr ratios. Therefore, Cr concentrations and evaluation of Ni/Cr or Co/Cr ratios in impact melts or spherules can be used to distinguish between iron and chondrite projectiles (Palme et al. 1978; Evans et al. 1993).

For the Lonar crater in particular, any form of iron meteorite or stony iron variant is unlikely as a candidate for the impactor. Geological investigations during the past century have failed to report any fragment of Fe-Ni metal phases from this crater in the field and in bore holes. Recent extensive petrographic and geochemical studies by Son and

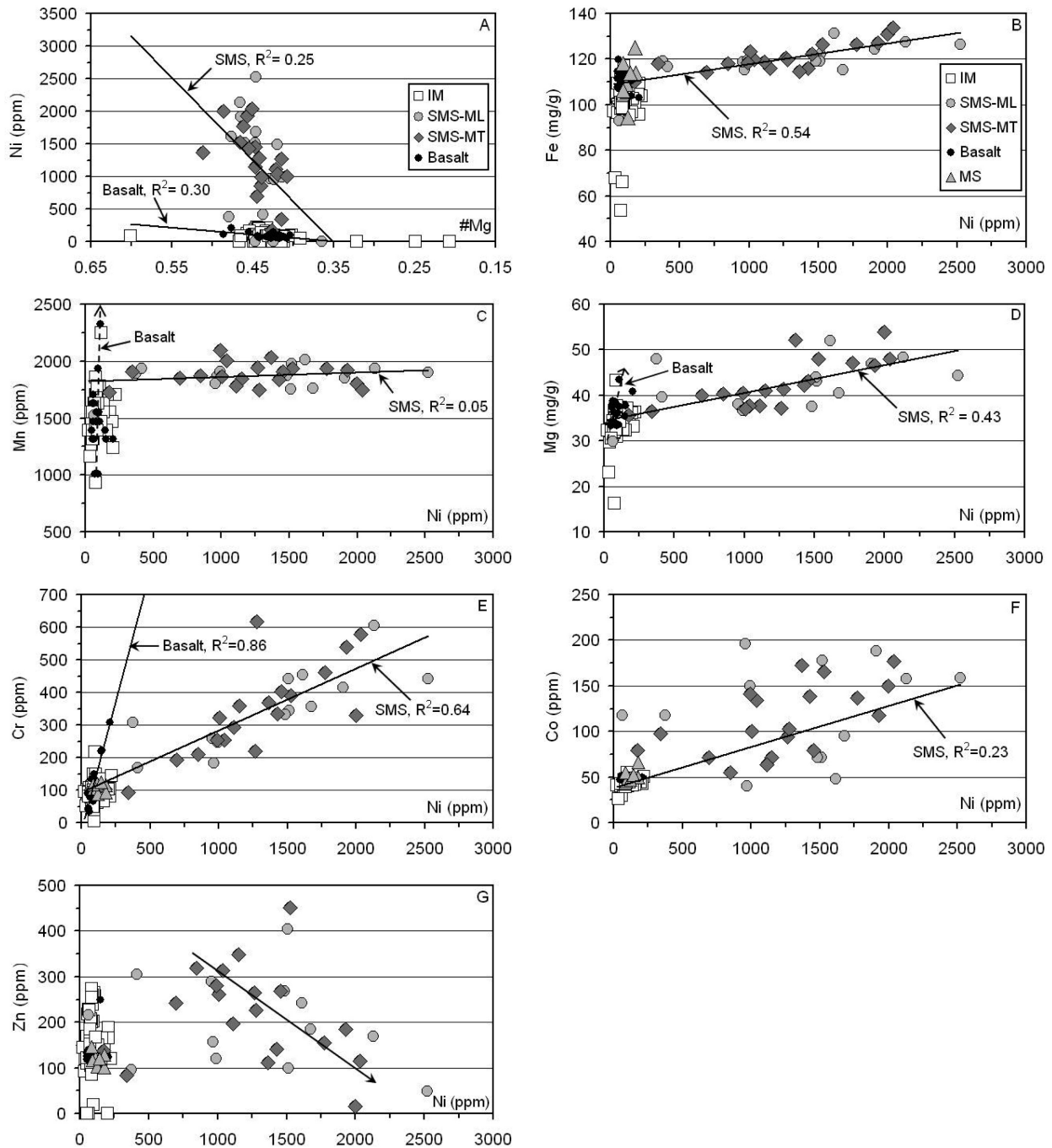


Fig. 5. Plots of Lonar samples in magnesium number (#Mg) or Ni versus major and trace element plots. Symbols: open square: impact melt (IM), light gray-colored circle: submillimeter-sized spherule with melt-dominated portion (SMS-ML), dark gray-colored rhombus: submillimeter-sized spherule with magnetite dominated portion (SMS-MT), black solid dot: target basalt, light gray-colored triangle: millimeter-sized spherule (MS). A) Ni shows a large variation from ~60 to 2500 ppm in the submillimeter-sized spherules. In target basalt and impact melts, Ni contents are low (~200 ppm), target basalts show a slight positive correlation with #Mg. In contrast, submillimeter-sized spherules have much higher Ni abundances showing positive correlation with #Mg, arguing against an igneous fractionation process to enrich the Ni. B–F) Ni (ppm) versus major or minor elements for Lonar samples. The element-Ni plots show correlations suggestive of mixing between the target composition and another component. The plots for Mn and Cr also show the strong correlations for target basalt compositions, with a very different slope from the spherule data, arguing against an igneous origin for the Cr-Ni correlation. G) Variation of Zn with Ni in Lonar samples, submillimeter-sized spherules show a linear negative correlation with Ni. Data from Osae et al. (2005), Son and Koeberl (2007), and Appendix.

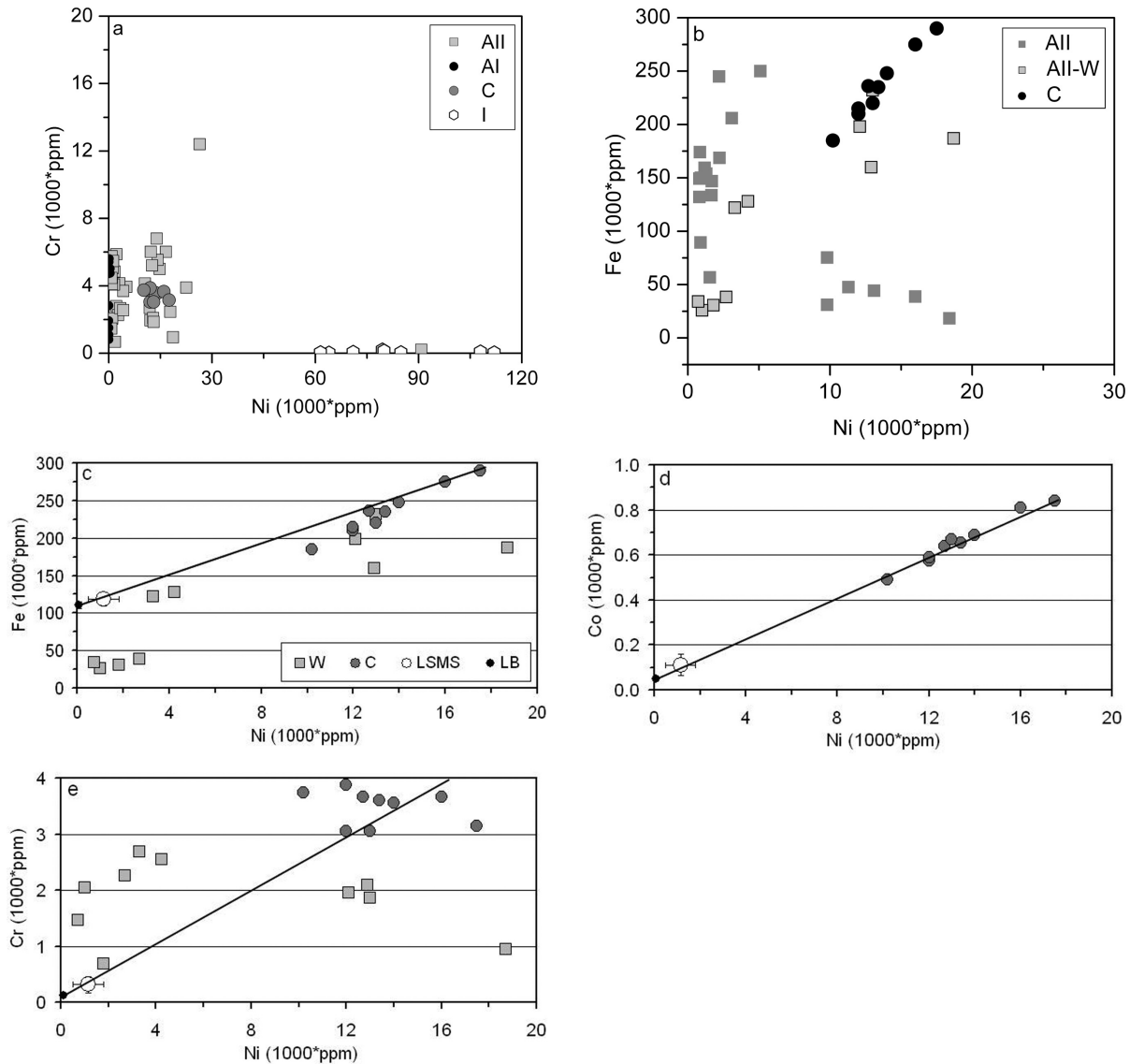


Fig. 6. a and b) Ni versus Cr and Fe discrimination plots showing fields of different meteorites: All- PGE-rich achondrite, AI- PGE-poor achondrite (after Tagle and Hecht 2006), All-W: winonaite; a variety of PGE-rich meteorite, C: chondrite, I: iron meteorite, data of achondrites and iron meteorites from Mittlefehldt et al. (1988), chondrites from Wasson and Kallemeyn (1988). c, d, e) Ni versus Fe, Cr and Co diagrams showing mixing trends between average Lobar basalt (LB), submillimeter-sized spherule (LSMS, error bars in diagrams showing percent standard deviations), chondrite (C) and winonaite (W). Target basalt data from Osae et al. (2005), submillimeter-sized spherule from Appendix, chondrite and winonaite as above.

Koeberl (2007) on 67 Lobar impactite and impact melt samples also have not identified any fragments of the impactor within these samples. The small ($\sim 150 \mu\text{m}$) opaque grains identified in some Lobar glasses/melts are magnetite and titanomagnetite and are interpreted as the remnants of target rock Deccan basalt. Therefore, the failure to identify any Fe-Ni metal phases from Lobar crater also argues against (but does not completely rule out) a pallasite, mesosiderite or other stony iron impactor for the Lobar crater. Mesosiderite meteorites are mixtures of metal containing approximately 8 wt% Ni and silicates with 0.5 to 1.5 wt% Cr_2O_3 , which are highly variable in metal content on the scale of several centimeters (Mittlefehldt et al. 1998). Depending on the

fraction of metal and silicate, essentially any Cr/Ni ratio is possible in a given fragment of mesosiderite. Therefore, it would require a remarkable coincidence that the contaminating material detected in each of the spherules represented fragments of mesosiderite with nearly identical metal/silicate ratios, which also happened to produce a chondritic Cr/Ni ratio.

Although bulk chemical composition is an important part of the classification system for meteorites (Wasson and Kallemeyn 1988; Krot et al. 2005; Weisberg et al. 2006), the elemental ratios for elements useful for impactor identification do not allow the discrimination of chondrite types (Tagle and Berlin 2008). Tagle and Hecht (2006)

discuss methods for determining the composition of impactor components in impact melt deposits. They advocate using a correlation method in the case of highly siderophile elements where the content of highly siderophile elements in the target is usually poorly known. Using this technique on the spherule Ni/Cr data (Appendix), a ratio of 3.1 is found that is well within the range in chondrites from 2.7 to 7.6. The situation for Co is different, however, because the concentrations in the target basalt are very well determined by bulk chemical techniques (Table 1), although the microprobe data for the spherules have substantial uncertainties. In particular, about half of the spherules have Co abundances between one and two sigma above the detection limit. Even with the uncertainties, the average Ni/Co ratio is 12 for most of the submillimeter-sized spherules (27 out of 33). When Ni and Co abundances of these spherules are corrected for the amounts contributed by the well-known abundances in the target basalt, the ratio rises to ~17, which is very close to the range in chondrites of 19 to 25 (Tagle and Berlin 2008).

Although a chondritic impactor fits the chemistry of the spherules, and is consistent with the preponderance of these meteorite types, we also consider the possibility that the impactor consisted of achondrite meteorites. The advantages and disadvantages of the identification of achondrite impactors by Ni, Cr and Fe, are as follows. The achondrites have recently been classified into two groups: PGE-poor achondrites (AI) including howardites, eucrites, and diogenites (HED), angrites and aubrites, and PGE-rich achondrites (AII), including brachinites, urelites, lodranites, acapulcoites and winonaites (Tagle and Hecht 2006). The Ni versus Cr plot shows that the AI achondrites, chondrites, and iron meteorites can clearly be distinguished in this variation diagram (Fig. 6a). The AI achondrites have low Ni concentrations and low Ni/Cr ratios; in contrast, the iron meteorites have low Cr concentrations and their Ni/Cr ratios are very high (cf. Mittlefehldt et al. 1998). The chondritic meteorites, however, which have both metal and silicate, have intermediate Ni/Cr ratios. The Ni-poor (5 mg/g) AII achondrites do not overlap with chondrites and are plotted close to the Cr-axis with AI achondrites but the Ni-rich variety of these achondrites show overlapping geochemistry with chondrites in this diagram. This problem of discrimination between impactors (at least for the Lonar spherules) can be easily overcome if the Ni versus Fe discrimination plot is also used (Fig. 6b). In this diagram, the Ni-poor AII achondrites show wide variation in Fe (between ~25 and 250 mg/g), but most of the Ni-rich AII achondrites have low Fe (75 mg/g). The chondrites show a distinct cluster for Fe that ranges between ~175 and 300 mg/g. Only a few (2) of the winonaite samples of AII achondrites, which are compositionally similar to the angular silicate inclusions present within IAB iron meteorites (cf. Mittlefehldt et al. 1988), overlap with the chondrite group.

In Fe, Co, and Cr versus Ni concentration diagrams, the average spherule data within error fall on a mixing line

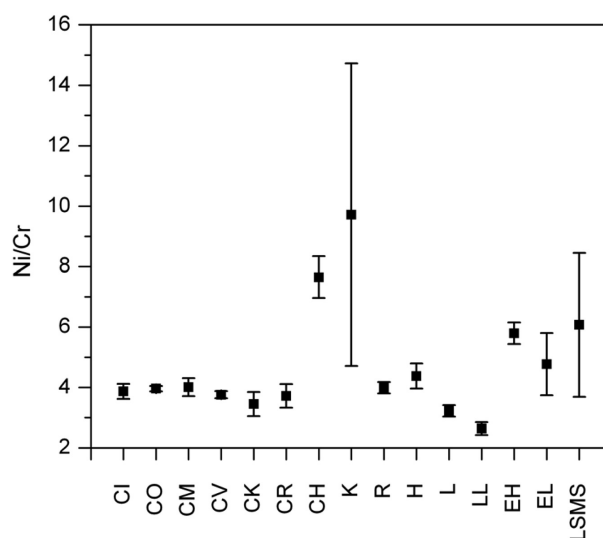


Fig. 7. Diagram showing variations of average Ni/Cr ratios in different types of chondrites (CI, CO, CM, CV, CK, CR, CH, K, R, H, L, LL, EH, EL) with error bars (data from Tagle and Berlin [2008]). The average Ni/Cr ratio for the Lonar submillimeter-sized spherules (LSMS), after correction for the average target basalt composition (data from Appendix and Osae et al. 2005, respectively), are consistent with EH type ordinary chondrites within our range of uncertainties.

between the average Lonar basalt and most of the average chondritic meteorite groups (Figs. 6c, 6d, and 6e). Most of the winonaites belonging to the AII achondrites have low or marginally elevated Fe compared to the Lonar target basalt and hence mixing of these impactor components with the Deccan Traps at Lonar cannot enrich the submillimeter-sized impact spherules in Fe. Most Ni-rich achondrites are also unlikely impactor candidates because they have Fe abundances that are far lower than those of Lonar target basalt (Figs. 6b and 6c), and hence mixing of these components with the Lonar basalts cannot enrich the magnetic spherules in Fe. In Ni versus Cr plots, any mixing line between target basalt and cluster of chondrites should include the average submillimeter-sized impact spherule within error (Fig. 6d). Other possible mixing lines through the target basalt and Winonaite compositions barely contain the submillimeter-sized magnetic spherules. Our conclusion from this assessment is that some type of chondrite may have been the most likely impactor for the Lonar crater. However, it is not possible to identify the specific chondrite group of impactor for the Lonar crater with the available data. Information on PGEs and their ratios are required for this purpose (McDonald et al. 2001; Tagle and Hecht 2006), which will be our next phase of research. However, Tagle and Berlin (2008) have recently determined the Ni/Ir, Co/Ir, Cr/Ir, and Ni/Cr ratios for different chondrite groups. When these data are compared with the Lonar magnetic spherules after corrections for the amounts contributed by the target basalt [i.e., $(\text{Ni}_{\text{spherule}} - \text{Ni}_{\text{average basalt}}) / (\text{Cr}_{\text{spherule}} - \text{Cr}_{\text{average basalt}})$], the average Ni/Cr ratio of these magnetic spherules is notably

higher than all the carbonaceous chondrite averages and close to the enstatite chondrite (EH type) (Fig. 7), although the uncertainties are very large. The use of Cr isotopic measurements and PGE determination will provide a more definitive answer in any case. Based on Ni concentrations, the maximum proportion of CI chondritic component that can be mixed with the target basalt melt to account for the high susceptibility spherules with the highest Ni (~2000 ppm, average of 6 analyses) is ~20 wt%. For an EH enstatite chondrite impactor representing chondrites with high Ni content, the fraction of meteorite material in the most enriched spherule is only 11%.

DISCUSSION

The identification of crater-forming projectiles allows the determination of the nature and frequency of bodies impacting the Earth with implications for future hazards due to asteroidal impact. The siderophile element data we report here, particularly Fe, Cr, and Ni enrichments in millimeter-sized impact spherules, suggest that the impactor that formed the Lonar crater is probably chondritic in composition. Our interpretation based on Fe, Cr, and Ni enrichments is consistent with chondritic signatures in other craters. For example, the impact melt rocks from the Morokweng impact structure, South Africa, which formed by impact of an ordinary (L or LL) chondrite, as proven by Cr-isotopic and PGEs studies, contain very high proportions of Cr (~70 times or more) and Ni (~33 times or more) over the target granite (McDonald et al. 2001). Currently, some ten impact craters with evidence for chondritic impactors are known (Tagle and Hecht 2006), and these range in size from Chicxulub (Mexico), ~180 km in diameter, down to New Quebec (Canada), ~3.4 km in diameter (cf. Koeberl 2007).

The distribution of meteoritic components between the impact melt clasts and spherules is also an important aspect of the evolution of Lonar crater. An important question is where the mixing of target rock melts and impactor components occurs in the generation of impact melts and spherules. As noted above, products of the Lonar impact event include impact melt clasts up to decimeters in size and spherules from submillimeter- to millimeter-size. Data for the bulk composition of the millimeter-sized spherules are presently very limited (cf. Osae et al. 2005; Son and Koeberl 2007). We interpret the results of our present study to suggest the definite presence of meteoritic components in submillimeter-sized impact spherules. The amount of chondritic material ranges up to 10 or 20 percent by mass. These results are similar to those obtained from the ~90 m diameter Wabar crater, Saudi Arabia, which was formed by impact of a IIIA iron meteorite on the quartz-dominated target ~6400 years ago. Aerodynamically shaped spherules (<1 cm in size) from the Wabar crater contain some 10 to 17 percent impactor component compared with less than 5 percent for the massive black and white melts found as chunks inside the crater

(Mittlefehldt et al. 1992). We interpret our observations on the products of formation of the Lonar crater to indicate that the submillimeter-sized impact spherules were quenched inside the expanding impact plume, which included at least a part of the vaporized impactor. The impact melt clasts, however, may have formed by shock or thermal heating in an environment separated from the projectile material incorporated into the ejecta plume. The total duration of the shock event producing the shock melting at Lonar crater specifically is suggested to be about 1 s (Kieffer et al. 1976). When the submillimeter-sized impact spherules solidified in the upper part of this plume, they incorporated the meteoritic components. During the formation of the plume and its expansion, the extreme mechanical and thermal environment and slightly different source materials from the target or impactor could have led to some of the observed chemical differences among the spherules.

CONCLUSIONS

Aerodynamically shaped Lonar impact spherules are of two types: millimeter-sized spherules with vesicular surface texture, and submillimeter-sized spherules with smoother surface morphology and high magnetic susceptibility. Both types of spherules possess high NRM intensities that are typically comparable to a SIRM, suggesting a very efficient remanence acquisition process. Progressive AF demagnetization typically reveals a non-linear yet systematic demagnetization trajectory, suggesting that remanence acquisition, likely by thermal blocking, took place while the spherules were in motion. Relatively low Na₂O and P₂O₅, and high Zn in the submillimeter-sized spherules compared to the target basalt abundances suggest exchange of volatiles between these spherules and surroundings within the impact plume.

The submillimeter-sized spherules contain correlated amounts of Cr and Ni that vary in abundances between about 100–600 and 200–2500 ppm, respectively. We conclude that these spherules were probably formed by mixing of target basalt melts and chondritic impactor material. Based on Ni abundances, the chondrite component in the submillimeter-sized spherules varied between ~12 and 20 weight percent. A chondritic impactor may be consistent with the absence of any meteorite fragments at Lonar, either due to disintegration of the impactor in the atmosphere (e.g., Boslough and Crawford, 2008) or the rapid post-impact weathering of meteorite fragments. The discovery of the evidence for a chondritic impactor at Lonar crater answers a mystery going back to the earliest history of impact crater studies (Gilbert 1896).

Acknowledgments—We are grateful to Christian Koeberl, Frank Kyte, and Roald Tagle for their constructive comments on the manuscript. We thank Mike Spilde for help with the electron microprobe. This research work was supported by NASA Planetary Geology and Geophysics program grant

NAG 5-11496 and NNX08AL74G to Horton Newsom, and by the Planetary Sciences and Exploration Program (PLANEX) of the Indian Space Research Organization, Bangalore, India (grant no. 9/1/194/2002-II) to D. Sengupta and S. Misra.

Editorial Handling—Dr. Christian Koeberl

REFERENCES

- Bland P. A. and Artemieva N. A. 2003. Efficient disruption of small asteroids by Earth's atmosphere. *Nature* 424:288–291.
- Bland P. A. and Artemieva N. A. 2006. The rate of small impacts on Earth. *Meteoritics & Planetary Science* 41:607–631.
- Boslough M. B. E. and Crawford D. A. 2008. Low-altitude airbursts and the impact threat. *International Journal of Impact Engineering* 35:1441–1448.
- Chakrabarti R. and Basu A. R. 2006. Trace element and isotopic evidence for Archean basement in the Lonar crater impact breccia, Deccan volcanic province. *Earth and Planetary Science Letters* 247:197–211.
- Chenet A.-L., Xavier Quidelleur X., Fluteau F., Courtillot V., and Bajpai S. 2007. ^{40}K – ^{40}Ar dating of the main Deccan large igneous province: Further evidence of KTB age and short duration. *Earth and Planetary Science Letters* 263:1–15.
- Chowdhury A. N., and Handa B. K. 1978. Some aspects of the geochemistry of Lonar lake water. *Indian Journal of Earth Sciences* 5:111–118.
- Cisowski S. 1981. Interacting versus non-interacting single domain behavior in natural and synthetic samples. *Physics of the Earth and Planetary Interiors* 26:56–62.
- Courtillot V., Gallet Y., Rocchia R., Féraud G., Robin E., Hofmann C., Bhandari N., and Ghevariya Z. G. 2000. Cosmic markers, $^{40}\text{Ar}/^{39}\text{Ar}$ dating and paleomagnetism of the K-T sections in the Anjar area of the Deccan large igneous province. *Earth and Planetary Science Letters* 182:137–156.
- Courtillot V. E. and Renne P. R. 2003. On the ages of flood basalt events. *Comptes Rendus Geoscience* 335:113–140.
- Earth Impact Database, <http://www.unb.ca/passc/ImpactDatabase>.
- Evans N. J., Gregoire D. C., Grieve R. A. F., Goodfellow W. D., and Veizer J. 1993. Use of platinum-group elements for impactor identification: Terrestrial impact craters and Cretaceous-Tertiary boundary. *Geochimica et Cosmochimica Acta* 57:3737–3748.
- Feldman V. I., Sazonova L. V., Mironov Y. V., and Kapustkina I. G. 1983. Circular structure Logancha as possible meteorite crater in basalts of the Tunguska syncline (abstract). 14th Lunar and Planetary Science Conference. pp. 191–192.
- Fredriksson K., Dube A., Milton D. J., and Balasundaram M. S. 1973. Lonar Lake, India: An impact crater in basalt. *Science* 180:862–864.
- Fredriksson K., Brenner P., Dube A., Milton D., Mooring C., and Nelen J. A. 1979. Petrology, mineralogy and distribution of Lonar (India) and lunar impact breccias and glasses. *Smithsonian Contributions to the Earth Sciences* 22:1–12.
- French B. M. 1998. *Traces of catastrophe*. LPI Contribution 954. Houston: Lunar and Planetary Institute. 120 p.
- Fudali R. F., Milton D. J., Fredriksson K., and Dube A. 1980. Morphology of Lonar crater, India: Comparisons and implication. *The Moon and the Planets* 23:493–515.
- Gattacceca J. and Rochette P. 2004. Toward a robust normalized magnetic paleointensity method applied to meteorites. *Earth and Planetary Science Letters* 227:377–393.
- Ghosh S. 2003. Is Lonar astrobleme an example of cometary impact? *Indian Minerals* 57:105–114.
- Ghosh S. and Bhaduri S. K. 2003. Petrography and petrochemistry of impact melts from Lonar crater, Buldana District, Maharashtra, India. *Indian Minerals* 57:1–26.
- Gilbert G. K. 1896. The origin of hypotheses, illustrated by the discussion of a topographic problem. *Science* 3:1–13.
- Grieve R. A. F. 1987. Terrestrial impact structures. *Annual Review of Earth and Planetary Sciences* 15:245–270.
- Grieve R. A. F. 1991. Terrestrial impact: The record in the rocks. *Meteoritics* 26:175–194.
- Gros J., Takahashi H., Hertogen J., Morgan J. W., and Anders E. 1976. Composition of the projectiles that bombarded the lunar highlands. Proceedings, 7th Lunar Science Conference. pp. 2403–2425.
- Hagerty J. J. and Newsom H. E. 2003. Hydrothermal alteration at the Lonar Lake impact structure, India: Implications for impact cratering on Mars. *Meteoritics & Planetary Science* 38:365–381.
- Hofmann C., Féraud G., and Courtillot V. 2000. $^{40}\text{Ar}/^{39}\text{Ar}$ dating of mineral separates and whole rocks from the Western Ghats lava pile: Further constraints on duration and age of the Deccan traps. *Earth and Planetary Science Letters* 180:13–27.
- Hörz F. 1965. Untersuchungen an Riesgläsern. *Beitrage zur Mineralogie und Petrographie* 11:621–661.
- Irvine T. N. and Baragar W. R. A. 1971. A guide to the chemical classification of the common volcanic rocks. *Canadian Journal of Earth Sciences* 8:523–548.
- Johnson H. P., Lowrie W., and Kent D. V. 1975. Stability of anhysteretic remanent magnetization in fine and coarse magnetite and maghemite particles. *Geophysical Journal of the Royal Astronomical Society* 41:1–10.
- Jarosewich E., Nelen J. A., and Norberg J. A. 1980. Reference samples for electron microprobe analysis. *Geostandards Newsletter* 4:43–47.
- Kearsley A., Graham G., McDonnell T., Bland P., Hough R., and Helps P. 2004. Early fracturing and impact residue emplacement: Can modeling help to predict their location in major craters? *Meteoritics & Planetary Science* 39:247–265.
- Kieffer S. W., Schaal R. B., Gibbons R., Hörz F., Milton D. J., and Dube A. 1976. Shocked basalt from Lonar impact crater, India, and experimental analogues. Proceedings, 7th Lunar Science Conference. pp. 1391–1412.
- Koeberl C. 1998. Identification of meteoritical components in impactites. In *Meteoritics: Flux with time and impact effects*, edited by Grady M. M., Hutchison R., McCall G. J. H., and Rothery D. A. Geological Society of London Special Publication 140. pp. 133–152.
- Koeberl C. 2007. The geochemistry and cosmochemistry of impacts. In: *Meteorites, comets, and planets*, edited by Davis A. Treatise on Geochemistry, vol. 1. Amsterdam: Elsevier. pp. 1–52, doi: 10.1016/B978-008043751-4/00228-5.
- Koeberl C., Bhandari N., Dhirga D., Suresh P. O., Narasimham V. L., and Misra S. 2004. Lonar impact crater, India: Occurrence of a basaltic suevite? (Abstract #1751). 35th Lunar and Planetary Science Conference. CD-ROM.
- Krot A. N., Keil K., Goodrich C. A., Scott E. R. D., and Weisberg M. K. 2005. Classification of meteorites. In: *Meteorites, comets, and planets*, edited by Davis A. M. Treatise on Geochemistry, vol. 1. Amsterdam: Elsevier. pp. 83–128.
- Kumar P. S. 2005. Structural effects of meteorite impact on basalt: Evidence from Lonar crater, India. *Journal of Geophysical Research* 110 (B12402), doi:10.1029/2005JB003662.
- Louzada K. L., Weiss B. P., Maloof A. C., Stewart S. T., and Swanson-Hysell N. 2007. A paleomagnetic study of Lonar

- impact crater, India (abstract #2344). 38th Lunar and Planetary Science Conference. CD-ROM.
- Mahoney J. J. 1988. Deccan Traps. In *Continental flood basalt*, edited by McDougall J. D. Dordrecht: Kluwer Academic Publishing, pp. 151–194.
- Masaitis V. L. 1999. Impact structures of northeastern Eurasia: The territories of Russia and adjacent countries. *Meteoritics & Planetary Science* 34:691–711.
- Master S. 1999. Evidence for an impact origin of the Amber lake structure: A smaller companion crater to Lonar impact crater, Maharashtra, India (abstract). *Meteoritics & Planetary Science* 34:A78.
- McDonald I., Andreoli M. A. G., Hart R. J., and Tredoux M. 2001. Platinum-group elements in the Morokweng impact structure, South Africa: Evidence for the impact of a large ordinary chondrite projectile at the Jurassic-Cretaceous boundary. *Geochimica et Cosmochimica Acta* 65:299–309.
- McDonald I., Peucker-Ehrenbrink B., Coney L., Ferriere L., Reimold W. U., and Koeberl C. 2007. Search for a meteoritic component in drill cores from the Bosumtwi impact structure, Ghana: Platinum group element contents and osmium isotopic characteristics. *Meteoritics & Planetary Science* 42:743–753.
- Misra S. 2006. Comments on 'Trace element and isotopic evidence for Archean basement in the Lonar crater impact breccia, Deccan volcanic province' by R. Chakrabarti and A. R. Basu in *Earth and Planetary Science Letters* 247:197–211. *Earth and Planetary Science Letters* 250:667–668.
- Misra S., Srivastava P. K., and Dube A. 2006a. Lonar impact crater, India: Did it form by oblique impact? (abstract #1085). 37th Lunar and Planetary Science Conference. CD-ROM.
- Misra S., Bose T., Newsom H. E., and Sengupta D. 2006b. Geochemistry of impact ejecta from Lonar crater, India: More clues to crater evolution (abstract #2123). 37th Lunar and Planetary Science Conference. CD-ROM.
- Mittlefehldt D. W., McCoy T. J., Goodrich, C. A., and Kracher A. 1998. Non-chondritic meteorites from asteroidal bodies. In *Planetary materials*, edited by Papike J. J. Reviews in Mineralogy, vol. 36. Washington, D. C.: Mineralogical Society of America, pp. 1–195.
- Mittlefehldt D. W., See T. H., and Hörz F. 1992. Dissemination and fractionation of projectile materials in the impact melts from Wabar crater, Saudi Arabia. *Meteoritics* 27:361–370.
- Morgan J. W. 1978. Lonar crater glasses and high-magnesium australites: Trace element volatilization and meteoritic contamination. Proceedings, 9th Lunar Science Conference. pp. 2713–2730.
- Morgan J. W., Higuchi H., Ganapathy R., and Anders E. 1975. Meteoritic material in four terrestrial meteorite craters. Proceedings, 6th Lunar Science Conference. pp. 1609–1623.
- Nandy N. C. and Dey V. B. 1961. Origin of the Lonar Lake and its alkalinity. *Journal of Tata Iron and Steel Company* 8:1–12.
- Nayak V. K. 1972. Glassy objects (impactite glasses?): A possible new evidence for meteoritic origin of the Lonar crater, Maharashtra state, India. *Earth and Planetary Science Letters* 14:1–6.
- Newsom H. E., Hagerty J. J., and Thorsos I. E. 2001. Location and sampling of aqueous and hydrothermal deposits in Martian impact craters. *Astrobiology* 1:71–88.
- Newsom H. E., Misra S., and Nelson M. J. 2007. Aqueous alteration of the proximal and distal ejecta blanket at Lonar crater, India (abstract #2056). 38th Lunar and Planetary Science Conference. CD-ROM.
- Osae S., Misra S., Koeberl C., Sengupta D., and Ghosh S. 2005. Target rocks, impact-glasses and melt rocks from the Lonar impact crater, India: Petrography and geochemistry. *Meteoritics & Planetary Sciences* 40:1473–1492.
- Palme H., Janssens M.-J., Takahashi H., Anders E., and Hertogen J. 1978. Meteorite material at five large impact craters. *Geochimica et Cosmochimica Acta* 42:313–323.
- Palme H., Göbel E., and Grieve R. A. F. 1979. The distribution of volatile and siderophile elements in the impact melt of East Clearwater (Quebec). Proceedings, 10th Lunar and Planetary Science Conference. pp. 2465–2492.
- Pande K., Pattanayak S. K., Subbarao K. V., Navaneethkrishnan P., and Venkatesan T. R. 2004. ^{40}Ar - ^{39}Ar age of a lava flow from the Bhimashankar Formation, Giravali Ghat, Deccan Traps. *Proceedings of Indian Academy of Science (Earth and Planetary Sciences)* 113:755–758.
- Rajasekhar R. P. and Mishra D. C. 2005. Analysis of gravity and magnetic anomalies over Lonar Lake, India: An impact crater in a basalt province. *Current Science* 88:1836–1840.
- Rao G. V. S. P. and Bhalla M. S. 1984. Lonar Lake: Paleomagnetic evidence of shock origin. *Geophysical Journal of the Royal Astronomical Society* 77:847–862.
- Rocholl A. B. E., Simon K., Jochum K. P., Bruhn F., Gehann R., Kramar U., Luecke W., Molzahn M., Pernicka E., Seufert M., Spettel B., and Stummeier J. 1997. Chemical characterization of NIST silicate glass certified reference material SRM 610 by ICP-MS, TIMS, LIMS, SSMS, INAA, AAS and PIXE. *Geostandards Newsletter* 21:101–114.
- Sengupta D., Bhandari N., and Watanabe S., 1997. Formation age of Lonar meteor crater, India. *Revista de Fisica Aplicada e Instrumentacao* 12:1–7.
- Sheth H. C. 2007. Plume-related regional prevolcanic uplift in the Deccan Traps: Absence of evidence, evidence of absence. In *Plates, plumes and planetary processes*, edited by Foulger G. R. and Jurdy D. M. GSA Special Paper 430. Boulder: Geological Society of America. pp. 785–803.
- Shoemaker E. M. 1977. Why study impact craters? In *Impact and explosion cratering: Planetary and terrestrial implication*, edited by Roddy D. J., Pepin R. O., and Merrill R. B. New York: Pergamon Press. pp. 1–10.
- Son T. H. and Koeberl C. 2007. Chemical variation in Lonar impact glasses and impactites. *GFF* 129:161–176.
- Stroube W. B. Jr., Grag A. N., Ali M. Z., and Ehmann W. D. 1978. A chemical study of the impact glasses and basalts from Lonar crater, India. *Meteoritics* 13:201–208.
- Storzer D. and Koeberl C. 2004. Age of the Lonar impact crater, India: First results from fission track dating (abstract #1309). 35th Lunar and Planetary Science Conference. CD-ROM.
- Tagle R. and Berlin J. 2008. A database of chondrite analyses including platinum group elements, Ni, Co, Au, and Cr: Implications for the identification of chondritic projectiles. *Meteoritics & Planetary Science* 43:541–559.
- Tagle R. and Hecht L. 2006. Geochemical identification of projectiles in impact rocks. *Meteoritics & Planetary Science* 41:1721–1735.
- Thakker C. D. and Ranade D. R. 2002. An alkalophilic Methanosarcina isolated from Lonar crater. *Current Science* 82:455–458.
- Wasson J. T. and Kallemeyn G. W. 1988. Compositions of chondrites. *Philosophical Transactions of the Royal Society of London A* 325:535–544.
- Weisberg M. K., McCoy, T. J., and Krot, A. N. 2006. Systematics and evaluation of meteorite classification. In *Meteorites and the early solar system II*, edited by Lauretta D. S. and McSween H. Y. Jr. Tucson: The University of Arizona Press. pp. 19–52.
- Weiss B. P., Garrick-Bethell I., Pedersen S., Maloof A. C., Louzada K. L., and Stewart S. T. 2007. Paleomagnetism of impact glass and spherules from Lonar crater, India (abstract #2360). 38th Lunar and Planetary Science Conference. CD-ROM.

- Widdowson M. and Mitchell C. 1999. Large-scale stratigraphical, structural and geomorphological constraints for earthquakes in the southern Deccan Traps, India: The case for denudationally driven seismicity. In *Deccan volcanic province*, edited by Subbarao K. V. Memoir Geological Society of India 43. pp. 425–452.
- Widdowson M., Pringle M. S., and Fernandez O. A. 2000. A post K-T boundary (early Palaeocene) age for Deccan-type feeder dykes, Goa, India. *Journal of Petrology* 41:1177–1194.
- Wignall P. B. 2001. Large igneous provinces and mass extinctions. *Earth Science Review* 53:1–33.
- Yakovlev O. I. and Basilevsky A. T. 1994. Experimental studies of geochemical aspects of impact cratering. In *Large meteorite impacts and planetary evolution*, edited by Dressler B. O., Grieve R. A. F., and Sharpton V. L. GSA Special Publication #293. Boulder: Geological Society of America. pp 73–80.

APPENDIX

Individual Microprobe Analyses of Lonar Submillimeter-Sized Impact Spherules

Analysis # ^a	1	2	3	4	5	6	7	8	9	10
Sample #	S1-A1	S1-A2	S3-A5	S4-A7	S5-A10	S8-A16	S9-A18	S10-A21	S11-A24	S11-A25
SiO ₂ (wt%)	48.27	45.11	46.22	47.68	48.01	47.81	49.12	50.02	49.41	49.80
TiO ₂	2.23	2.27	2.51	2.11	2.27	2.18	2.95	2.34	2.42	2.37
Al ₂ O ₃	13.70	13.54	15.21	12.48	12.95	13.81	13.74	13.29	13.82	13.47
Fe ₂ O ₃	17.07	18.77	16.71	18.22	17.47	17.02	17.08	16.51	16.98	17.09
MnO	0.24	0.26	0.25	0.25	0.26	0.23	0.21	0.24	0.23	0.25
MgO	7.94	8.62	6.56	8.00	7.13	7.30	4.95	6.24	6.30	6.08
CaO	8.98	9.53	10.20	8.67	9.59	8.98	8.72	9.07	8.64	8.73
Na ₂ O	1.23	1.33	1.87	1.76	1.67	1.92	2.28	1.81	1.67	1.68
K ₂ O	0.19	0.21	0.31	0.31	0.32	0.33	0.78	0.28	0.26	0.30
P ₂ O ₅	0.02	0.06	0.03	0.13	0.05	0.09	0.15	0.02	0.04	0.04
Total	99.88	99.69	99.88	99.60	99.72	99.68	99.96	99.83	99.78	99.80
#Mg	0.48	0.48	0.44	0.47	0.45	0.46	0.36	0.43	0.42	0.41
Cr (ppm)	307	455	169	605	344	440	27	183	259	247
Co (ppm)	118	48	BDL	158	178	71	70	40	196	150
Ni (ppm)	376	1614	412	2131	1517	1509	BDL	968	956	993
Zn (ppm)	96	243	306	169	99	404	239	157	289	121

Analysis # ^a	11	12	13	14	15	16	17	Melt-rich zone n = 17	
								Average	S.d.
Sample #	S12-A26	S13-A28	S14-A30	S16-A34	S17-A37	S18-A38	S18-A39		
SiO ₂ (wt%)	51.39	51.39	50.24	51.18	48.00	49.37	49.54	48.97	1.74
TiO ₂	2.10	2.15	2.15	2.26	2.18	1.94	2.27	2.28	0.22
Al ₂ O ₃	15.23	14.46	12.86	14.81	12.77	11.76	12.96	13.58	0.95
Fe ₂ O ₃	13.29	13.61	16.50	13.80	17.78	18.09	17.06	16.65	1.59
MnO	0.20	0.21	0.23	0.18	0.24	0.25	0.24	0.23	0.02
MgO	4.96	5.54	6.71	5.14	7.78	7.36	6.21	6.64	1.11
CaO	9.70	9.85	8.67	9.45	8.88	8.21	9.16	9.12	0.52
Na ₂ O	2.38	2.21	1.99	2.32	1.73	2.14	1.82	1.87	0.33
K ₂ O	0.62	0.51	0.32	0.68	0.27	0.42	0.35	0.38	0.17
P ₂ O ₅	0.06	0.05	0.03	0.09	0.05	0.07	0.10	0.06	0.04
Total	99.94	99.96	99.70	99.92	99.67	99.59	99.72	99.78	0.12
#Mg	0.43	0.45	0.45	0.42	0.46	0.45	0.42	0.44	0.03
Cr (ppm)	96	150	357	116	416	441	332	291	155
Co (ppm)	118	63	95	165	188	158	71	118	53
Ni (ppm)	BDL	BDL	1677	BDL	1909	2523	1483	1295	703
Zn (ppm)	217	96	185	344	BDL	49	268	205	101

Analysis # ^a	18	19	20	21	22	23	24	25	26	27
Sample #	S1-A3M	S3-A4M	S3-A6M	S4-A8M	S5-A9M	S6-A11M	S6-A12M	S7-A13M	S7-A14M	S8-A15M
SiO ₂ (wt%)	47.28	46.80	47.83	47.62	48.31	47.48	48.33	48.36	46.94	49.18
TiO ₂	2.21	2.54	2.51	2.17	2.32	2.30	2.38	2.50	2.52	2.22
Al ₂ O ₃	13.14	15.13	14.27	12.63	13.82	13.68	13.86	14.87	14.32	13.20
Fe ₂ O ₃	18.11	16.36	16.88	18.18	16.61	17.47	17.02	15.77	16.90	16.62
MnO	0.25	0.24	0.24	0.25	0.24	0.25	0.23	0.22	0.25	0.24
MgO	7.96	6.63	6.69	7.71	6.79	7.14	6.25	5.91	6.04	7.00
CaO	9.17	10.04	9.45	8.67	9.59	9.15	9.42	10.12	10.71	8.75
Na ₂ O	1.30	1.80	1.63	2.01	1.69	1.83	1.89	1.86	1.87	2.12
K ₂ O	0.22	0.25	0.26	0.32	0.30	0.33	0.33	0.32	0.32	0.31
P ₂ O ₅	0.03	0.05	0.05	0.09	0.08	0.08	0.08	0.03	0.06	0.10
Total	99.67	99.84	99.81	99.64	99.75	99.71	99.78	99.94	99.92	99.73
#Mg	0.47	0.44	0.44	0.46	0.45	0.45	0.42	0.43	0.41	0.45
Cr (ppm)	390	192	210	539	359	402	292	103	92	334
Co (ppm)	165	71	55	118	71	80	64	79	98	138
Ni (ppm)	1526	694	848	1929	1150	1456	1111	174	342	1426
Zn (ppm)	450	242	318	184	349	268	196	137	83	141

Analysis # ^a	28	29	30	31	32	33	34	35	36	Magnetite-rich zone n = 19	
										Avg	S.d.
Sample #	S10-A19M	S10-A20M	S10-A22M	S10-A23M	S14-A31M	S15-A32M	S15-A33M	S17-A35M	S17-A36M		
SiO ₂ (wt%)	47.99	49.23	48.54	47.98	48.37	43.33	47.78	46.60	47.35	47.65	1.27
TiO ₂	2.39	2.38	2.34	2.42	2.29	2.52	2.20	2.25	2.21	2.35	0.12
Al ₂ O ₃	14.82	13.74	13.74	14.52	12.99	14.72	13.06	12.15	12.69	13.76	0.85
Fe ₂ O ₃	17.17	17.27	17.66	16.96	17.15	18.72	16.37	19.14	18.08	17.29	0.86
MnO	0.26	0.25	0.24	0.27	0.23	0.23	0.26	0.23	0.25	0.24	0.01
MgO	6.26	6.17	6.14	6.70	6.87	8.93	8.65	7.95	7.82	7.03	0.90
CaO	8.84	8.59	8.78	9.08	9.56	9.56	9.69	9.24	9.19	9.35	0.55
Na ₂ O	1.70	1.79	1.89	1.57	1.73	1.42	1.46	1.68	1.75	1.74	0.20
K ₂ O	0.29	0.31	0.30	0.22	0.36	0.19	0.20	0.28	0.26	0.28	0.05
P ₂ O ₅	0.06	0.05	0.14	0.05	0.16	0.03	0.04	0.11	0.07	0.07	0.04
Total	99.77	99.76	99.78	99.78	99.71	99.68	99.74	99.62	99.67	99.75	
#Mg	0.42	0.41	0.41	0.44	0.44	0.49	0.51	0.45	0.46	0.44	0.03
Cr (ppm)	253	219	323	253	618	329	369	579	461	333	146
Co (ppm)	134	94	101	142	103	150	173	176	137	113	38
Ni (ppm)	1038	1265	1005	990	1278	1998	1365	2035	1773	1232	512
Zn (ppm)	314	265	261	281	226	16	112	115	156	217	105

^aAnalysis numbers 1–17 include melt-rich portions of spherules, analysis numbers 18–36 include magnetite-rich portions of spherules, #Mg is the magnesium number [mole MgO/(mole MgO + mole FeO²⁺)]. All major oxide data are reported to two significant figures after decimal, trace elements numbers are rounded off. BDL = below detection limit, n = number of analyses, S.d. = standard deviation.